Article type: ((**Full Paper**))

Optimization of the thermoelectric properties of p-type $Mg_{2-y}Li_yGe_{1-x}Sn_x$ and $Mg_{2-y}Li_yGe_{1-z}Si_z$ with x,z = 0.1 and 0.2.

Vidushi Galwadu Arachchige, Hasbuna Kamila*, Aryan Sankhla, Léo Millerand, Silvana Tumminello, Kunal Mitra, Mohammad Yasseri, Eckhard Müller, and Johannes de Boor**

Vidushi Galwadu Arachchige[a,b], Hasbuna Kamila[a], Aryan Sankhla[a], Léo Millerand[a,e], Dr. Silvana Tumminello[a], Kunal Mitra[a], Mohammad Yasseri[a,c], Prof. Eckhard Müller [a,c], and Jun. Prof. Johannes de Boor[a,d]

[a] Institute of Materials Research, German Aerospace Center (DLR), 51147 Cologne, Germany

[b] Department of Chemistry and Pharmacy, Friedrich - Alexander Universität, 91058 Erlangen, Germany

[c] Institute of Inorganic and Analytical Chemistry, Justus Liebig University Giessen, 35392 Giessen, Germany

[d] Faculty of Engineering, Institute of Technology for Nanostructures, University of Duisberg - Essen, 47057

[e] European Astronaut Centre, European Space Agency, Linder Hoehe, 51147 Cologne, Germany

E-mail: Vidushi.galwadu@gmail.com, Hasbuna.kamila@dlr.de, and Johannes.deboor@dlr.de

Abstract

According to recent investigations on p-type Mg_2X (X = Si, Sn, Ge), p-type Mg_2Ge is found to be far superior to the p-type binaries while having thermoelectric properties comparable to the best solid solutions of p-type $Mg_2(Si,Sn)$. The unexpectedly good properties are supposedly due to a non-rigid band structure with a temperature dependent interband separation. Further optimization can be expected by alloying Si or Sn into the Ge site to lower the thermal conductivity thereby increasing the figure of merit. Here, solid solutions of p-type $Mg_2Ge_{1-x}Sn_x$ and p-type $Mg_2Ge_{1-z}Si_z$ with x, z = 0.1 and 0.2 are successfully synthesized via ball milling. The thermal conductivities

are significantly reduced throughout the whole temperature range by around 30% due to the alloying effect. The electronic properties of all Ge-rich samples show similar temperature dependent behavior as p-type Mg_2Ge. For the $Mg_2(Ge,Sn)$ systems, a compensation of reduced thermal conductivity and decreased carrier mobility are found, leading to zT values comparable to p-type Mg_2Ge. Whereas for the Si containing samples, a thermoelectric figure of merit zT of 0.49±0.07 at 675 K for $z = 0.1$ is achieved, the highest reported so far for the p-type $Mg_2(Ge,Si)$ systems and a zT_{avg} which is 30% higher than that of binary Mg_2Ge.

Keywords: Synthesis, ball milling, p-type $Mg_2Ge_{1-z}Si_z$ solid solutions, p-type $Mg_2Ge_{1-x}Sn_x$ solid solutions, thermoelectric properties, microstructure

1. Introduction

In the present day and time, global climate change has become a topic spoken in every corner of the world. Due to the increasingly alarming impacts of fossil fuels on the environment, a significant reduction of greenhouse gases defines the energy challenge in the current world. Apart from direct approaches involving harvesting wind and solar energy, strategies to improve energy usage efficiency are also being developed, including the recovery and direct conversion of waste heat to electrical energy using thermoelectric (TE) materials. The advantages of thermoelectric modules over other heat recovery technologies include the absence of moving parts, high reliability, and low maintenance costs [1].

Thermoelectric performance is characterized by the dimensionless figure of merit, $zT = \frac{S^2 \sigma T}{\kappa}$ where S is the Seebeck coefficient, σ is the electrical conductivity, κ is the thermal conductivity and T is the temperature. The figure of merit zT can be optimized by increasing the thermoelectric

power factor ($S^2\sigma$) and decreasing κ. The TE power factor can be maximized by an optimization of the carrier concentration (p) (linked to both S and σ) [2] and advanced strategies like band structure engineering [3-6]. In contrast, the thermal conductivity can be brought down by strategies such as alloying [4, 7-8].

Among various thermoelectric materials [8-13], Mg_2X (X = Si, Sn, and Ge) and its solid solutions have attracted attention due to their non-toxicity, material abundance, and good environmental compatibility. The n-type Mg_2(Si, Ge, Sn) materials are known for their excellent thermoelectric properties [4, 7, 14-15], while the corresponding p-type is found to have inferior properties [16-19]. This is mainly due to the less favorable properties of the valence bands compared to the conduction bands [16-17, 20]. However, to produce efficient thermoelectric modules, it is important to optimize both p-type and n-type materials. Recent systematic investigations identify the optimum properties for p-type Mg_2(Si, Sn) with $zT \approx 0.5$ at 700 K and further improvement, e.g., by refined synthesis approaches is challenging [16, 21].

Recently, p-type Mg_2Ge was found to have zT values comparable to optimized p-type $Mg_2Si_{1-x}Sn_x$ ($zT \approx 0.5$) [20] and the highest zT among the p-type binaries reported in the literature [16, 22-24]. The better thermoelectric properties are attributed to a non-rigid band structure with a temperature dependent interband separation. The second band contributes progressively to the transport properties as the temperature increases thus leading to a higher power factor compared to p-type Mg_2Si and Mg_2Sn [20]. Further improvement of the properties is plausible by alloying and forming Mg_2Ge based solid solutions for a reduction of lattice thermal conductivity similar to Mg_2(Si, Sn)[16].

Here, in this study, the syntheses of p-type $Mg_2Ge_{1-x}Sn_x$ and $Mg_2Ge_{1-z}Si_z$ with $x, z = 0.1$ and 0.2 is carried out via high energy ball milling using Li as a dopant. The results reveal that the addition of Si and Sn into the Mg_2Ge system reduces the thermal conductivity. However, with decreasing Ge content, we observe an increasing secondary phase content that might be detrimental for the carrier mobility. Furthermore, for alloying with Mg_2Si we find a systematic decrease of the achievable carrier concentration, limiting the power factor. The best thermoelectric properties were found for $z = 0.1$ with a $zT_{\max}$ comparable to that of Mg_2Ge but an average figure of merit which is approximately 30% higher.

2. Materials and methods

$Mg_{2-y}Li_yGe_{1-x}Sn_x$ and $Mg_{2-y}Li_yGe_{1-z}Si_z$ with $x, z = 0.1$ and 0.2 and $y = 0.01, 0.02, 0.03$ and 0.05 were synthesized via high energy ball milling and direct current sinter pressing. In addition, $y = 0.01$ and 0.05 were prepared for the $z = 0.1$. To obtain a homogenous fine powder for the sintering process, mechanical alloying using a SPEX 8000D series Mixer/Mill was carried out for a total of 3 to 4 hours, depending on the composition. A total of 10 grams of the elements, Mg turnings (Merck), Si (< 6mm, Chempure), Sn (< 71 μm, Merck), Ge (polycrystalline 99%), and Li granules (with purity > 99.5%) were weighted according to nominal composition and loaded into a stainless steel jar along with stainless steel balls (purchased from SPEX) in an Argon glove box. During the milling step, the powders were checked every hour to get any agglomerates off the jar walls. At the final step, if any agglomerates were present, the powders were milled again for a time period of 6 to 18 minutes. No massive mechanical force must be applied to remove the agglomerates since this can result in the burning of the powders, possibly due to the presence of Lithium and Germanium together [20]. The whole procedure was done inside the glovebox including the removal of agglomerations from the jar walls after 1 hour of milling. For the completion of

reaction to obtain the desired phase with good densification, the powder was loaded in a graphite die of diameter 12.7 mm and sintered using a direct current sintering press (DSP 510 SE) from Dr. Fritsch GmbH at 973 K for $Mg_2Ge_{1-z}Si_z$ and 923 K for $Mg_2Ge_{1-x}Sn_x$ under vacuum (10^{-5} bar) with a holding time of 10 minutes, and under a sintering pressure of 66 MPa with a heating rate 1 K/s [20, 25]. The densities of the pellets were measured using the Archimedes method, and the relative densities of the obtained pellets were found to be > 97% of the theoretical values. The samples with $z = 0.2$ exhibit poor chemical stability under ambient conditions and developed a green oxide layer on the surface of the pellets complicating thermoelectric transport measurements. The pellets were therefore kept inside the glove box or sealed vacuum bags and taken outside only directly before the measurements.

The temperature dependent Seebeck coefficient and electrical conductivity were measured using an in house developed measurement system with an error bar of $\pm 5\%$ [26-27]. The thermal diffusivity (α) was measured using Netzsch LFA 427 (Laser Flash Apparatus) and Netzsch LFA 467 HT Hyperflash setups. The obtained values are used to calculate the thermal conductivity with an error bar $\pm 8\%$ by using the relation $\kappa = \alpha C_p \rho$, where ρ and C_p correspond to the density of sample and linear heat capacity. C_p is calculated by using the Dulong-Petit approximation, C_V^{DP}: $C_p = C_V^{DP} + \frac{9E_t^2 T}{\beta_T \rho}$ where $E_t \approx 1.6 \times 10^{-5} - 2 \times 10^{-6} z$ K^{-1}, $E_t \approx 1.6 \times 10^{-5} + 2 \times 10^{-6} x$ K^{-1} and $\beta_T \approx 1.7 \times 10^{-11}$ Pa, $\beta_T \approx 1.7 \times 10^{-11} + 7.029 \times 10^{-12} x$ Pa, are the linear coefficients of thermal expansion and linear isothermal compressibilities, respectively for $Mg_{2-y}Li_yGe_{1-z}Si_z$ and $Mg_{2-y}Li_yGe_{1-x}Sn_x$ [16, 20, 28]. Thermal cycling data for two selected samples is shown in Figure S2. The samples can show a minor change within the first measurement cycle but are stable afterwards, in line with earlier observations on Li-doped Mg_2(Si,Sn,Ge) samples [16, 20, 25]. The transport properties of all samples which are presented here are the cooling data measured during thermal cycling. For the compositional analysis, X-ray diffraction (XRD) data was obtained using a Bruker's D8-Advanced diffractometer in the 2θ range of 20° to 80° while using Cu Kα radiation. Rietveld analysis was performed using TOPAS [29] on the XRD patterns. Moreover, Scanning Electron

Microscopy was done using a Zeiss Ultra 55 along with Energy dispersive spectroscopy (EDX) to obtain information on the local composition from different areas of the sample. Hall measurements were performed using an in-house facility with a van der Pauw configuration under a varying magnetic field of max. $\pm$0.5 T with an estimated uncertainty of 10% [30]. The Hall carrier concentration (p_{H}) was calculated from the Hall coefficient (R_{H}) assuming a single carrier type using the relation $p_{\mathrm{H}} = \frac{1}{R_{\mathrm{H}}\, e}$ where e denotes an electron's charge. This serves as a rough estimate for the carrier concentration, even though two hole types likely contribute to the transport [20] and the assumption of a SPB model is therefore not strictly valid, see discussion in [31]. This also implies that the obtained mobilities are effective values.

3. Results

3.1 Microstructure

The XRD patterns are indexed to the anti-flourite cubic crystal structure with space group Fm-3m (ICSD collection code #81735 for Mg_2Ge). The XRD patterns depict the main phase peaks with some secondary phases but no traces of MgO (ICSD collection code #158103) for both z = 0.1 and z = 0.2 as shown in **Figure 1a.**

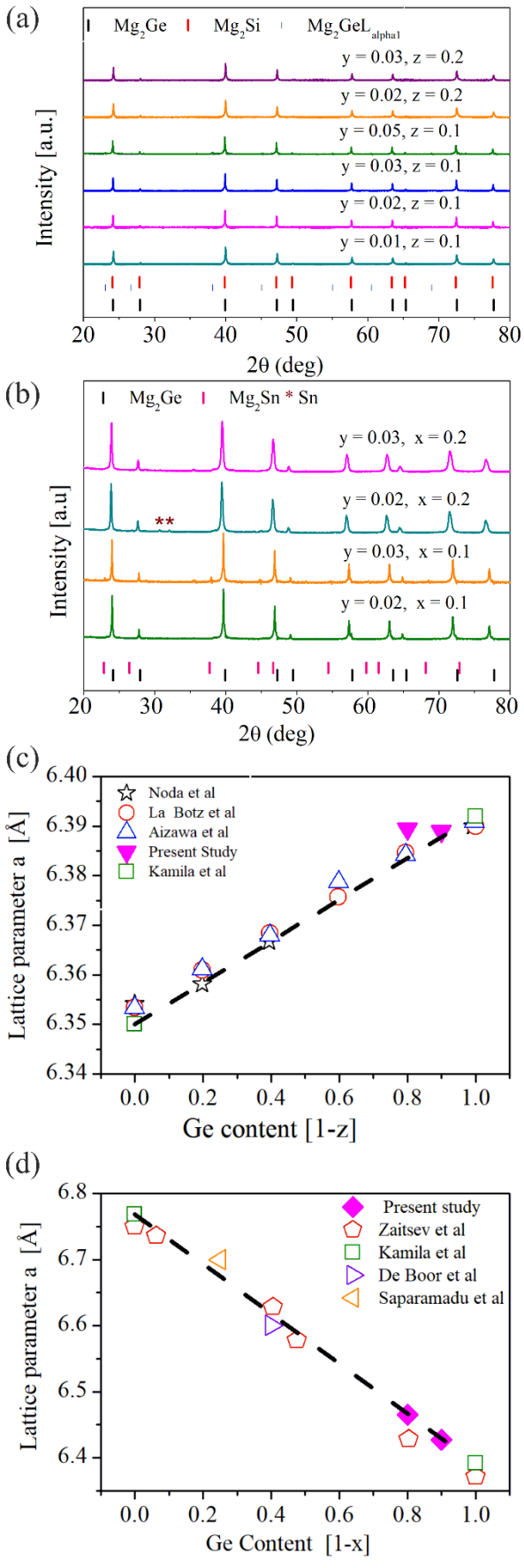
(a)
Mg2Ge
Mg2Si
Mg2GeLalpha1
y = 0.03, z = 0.2
y = 0.02, z = 0.2
y = 0.05, z = 0.1
y = 0.03, z = 0.1
y = 0.02, z = 0.1
y = 0.01, z = 0.1
Intensity [a.u.]
2θ (deg)
(b)
Mg2Ge
Mg2Sn * Sn
y = 0.03, x = 0.2
y = 0.02, x = 0.2
**
y = 0.03, x = 0.1
y = 0.02, x = 0.1
Intensity [a.u]
2θ (deg)
(c)
Noda et al
La Botz et al
Aizawa et al
Present Study
Kamila et al
Lattice parameter a [Å]
Ge content [1-z]
(d)
Present study
Zaitsev et al
Kamila et al
De Boor et al
Saparamadu et al
Lattice parameter a [Å]
Ge Content [1-x]

Figure 1 XRD patterns of the pellets (a) $Mg_{2-y}Li_yGe_{1-z}Si_z$ and (b) $Mg_{2-y}Li_yGe_{1-}$ with x, z = 0.1 and 0.2 for y = 0.02 and 0.03. y = 0.01 and 0.05 is for $z = 0.1$. Note that in (a) also the peaks corresponding to the $L_{\alpha 1}$ of Mg_2Ge from a tungsten source are indicated. (c) and (d) Comparison of the respective lattice parameters with literature [19-20, 25, 32-36] with the black dashed line correspond to Vegard's law.

The impurity peaks for $y = 0.05$ are Mg_2GeL_{alpha1}; this is due to tungsten contamination that evaporates from the cathode and gets deposited on the copper anode [37]. No elemental Si is observed in the XRD patterns; however, due to the similarities between the XRD patterns of the binaries Mg_2Si (ICSD collection code #192556) and Mg_2Ge and the solid solutions, it is not possible to deduce for $Mg_2(Ge,Si)$ if the synthesis was successful from the XRD pattern alone. The XRD patterns for x = 0.1 and x = 0.2 also depict the main phase peaks with some secondary phases but no traces of MgO as shown in **Figure 1**(b). Elemental impurities of Sn (ICSD collection code #106072) were found at $2\Theta = 30.72^o$ and $2\Theta = 32.13^o$ for x = 0.2 and y = 0.02. The presence of elemental impurities suggests a possible need to increase the milling time and the observation of Mg_2Sn may indicate that Mg_2Ge is thermodynamically more favorable as compared to Mg_2Sn. Rietveld refinement was performed on the pellet XRD data with the TOPAS software. The secondary phases and the refined lattice parameters are given in Table 1. The lattice constants were estimated to be $a = 6.388 - 6.391$ Å and $a = 6.389$ Å for $z = 0.1$ and 0.2 respectively and a = 6.427 Å and $a = 6.465$ Å for x = 0.1 and 0.2, respectively; in **Figure 1** mean of lattice constants of samples with different y are shown. For z = 0.1 and x = 0.1, 0.2, the estimated lattice constants are not far off from the literature values, whereas with z = 0.2 a larger discrepancy is observed. This is possibly due to the presence of several secondary phases in the systems.

For further analysis Rietveld refinement using TOPAS was carried out and a goodness of fit in the range of 2 – 4 was obtained for all samples (Table S1). Secondary phases corresponding to Mg_2Ge, Mg_2Si, $Mg_2Ge_{0.46}Si_{0.16}$, and $Mg_2Ge_{0.88}Si_{0.09}$ were found for $z = 0.2$. For all other samples the

Rietveld refinement estimated lattice constants close to those expected for the nominal composition.

Table 1 Rietveld refinement data for $Mg_{2-y}Li_yGe_{1-z}Si_z$ and $Mg_{2-y}Li_yGe_{1-x}Sn_x$ with x, z = 0.1 and 0.2 for y = 0.02 and 0.03. $y =$ 0.01 and 0.05 is only for $z = 0.1$.

Nominal composition	**Lattice constant (Å)**	**Secondary phases**
$Mg_{1.99}Li_{0.01}Ge_{0.9}Si_{0.1}$	6.389	-
$Mg_{1.98}Li_{0.02}Ge_{0.9}Si_{0.1}$	6.388	-
$Mg_{1.97}Li_{0.03}Ge_{0.9}Si_{0.1}$	6.388	-
$Mg_{1.95}Li_{0.05}Ge_{0.9}Si_{0.1}$	6.391	-
$Mg_{1.98}Li_{0.02}Ge_{0.8}Si_{0.2}$	6.390	Mg_2Ge (7%)
		Mg_2Si (22.7%)
$Mg_{1.97}Li_{0.03}Ge_{0.8}Si_{0.2}$	6.389	$Mg_2Ge_{0.46}Si_{0.16}$ (27.2%)
		Mg_2Si (9.8%)
$Mg_{1.98}Li_{0.02}Ge_{0.9}Sn_{0.1}$	6.428	
$Mg_{1.97}Li_{0.03}Ge_{0.9}Sn_{0.1}$	6.426	
$Mg_{1.98}Li_{0.02}Ge_{0.8}Sn_{0.2}$	6.465	Sn (1.2%)
$Mg_{1.97}Li_{0.03}Ge_{0.8}Sn_{0.2}$	6.465	

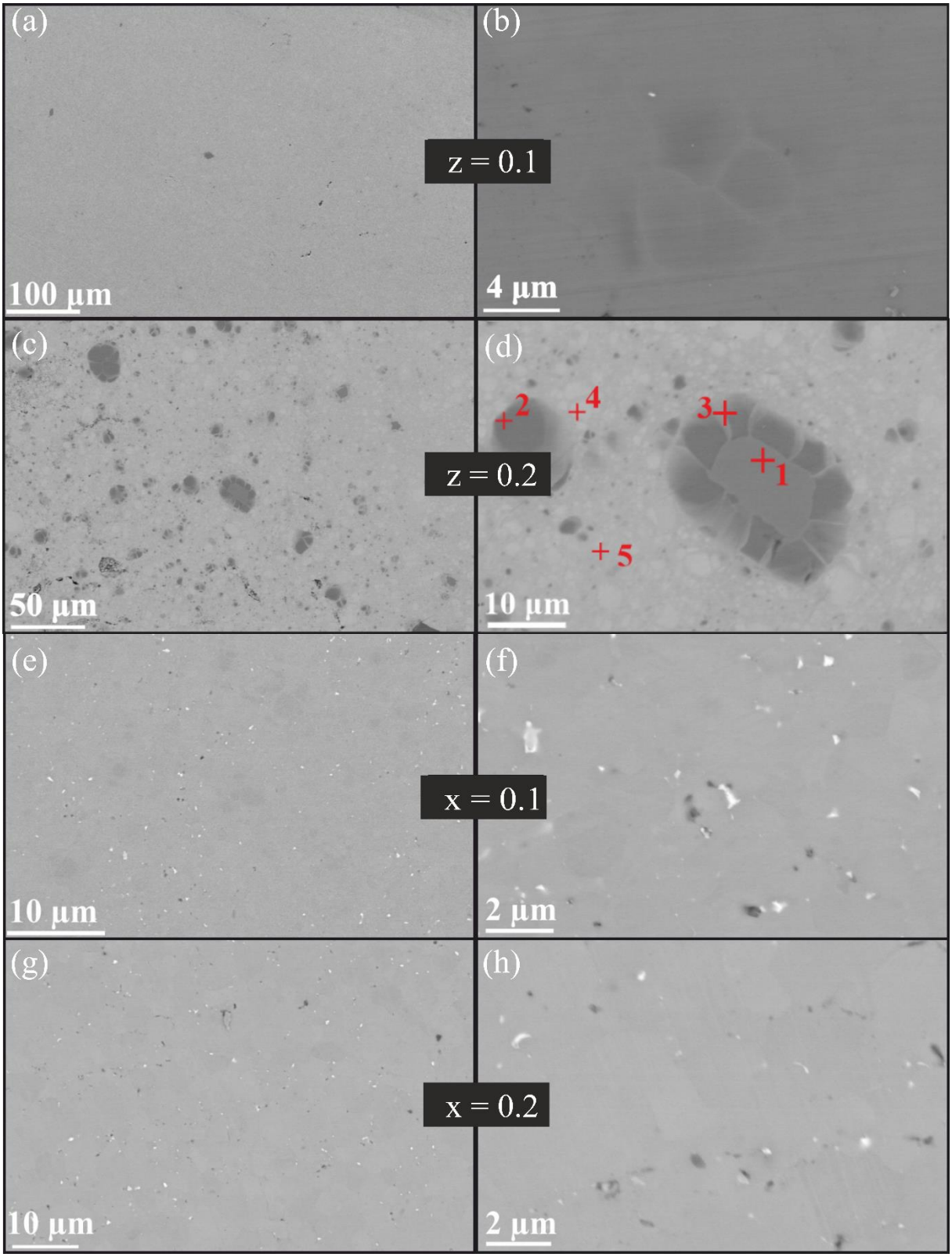

Figure 2 SEM-BSE images of (a-b) $Mg_{1.97}Li_{0.03}Ge_{0.9}Si_{0.1}$, (c-d) $Mg_{1.98}Li_{0.02}Ge_{0.8}Si_{0.2}$, (e-f) $Mg_{1.98}Li_{0.02}Ge_{0.9}Sn_{0.1}$,

(g-h) $Mg_{1.98}Li_{0.02}Ge_{0.8}Sn_{0.2}$ with left and right showing low and high magnification images, respectively. The marked points are given in Table 2.

Table 2 EDX point analysis for $Mg_{2-y}Li_yGe_{1-z}Si_z$ with $z = 0.2$ and $y = 0.02$

Number	Mg (at%)	Ge (at%)	Si (at%)	Phase (approximately)
1	0.5	0.1	99.4	Si
2	66.6	0.1	33.3	Mg_2Si
3	68.2	7.4	24.4	$Mg_2Ge_{0.3}Si_{0.7}$
4	70.8	28.4	0.8	Mg_2Ge
5	71.1	24.2	4.7	$Mg_2Ge_{0.9}Si_{0.1}$

The SEM images depict homogeneous distribution of precipitates for $z = 0.1$, $x = 0.1$ and 0.2, whereas with $z = 0.2$ some secondary phases are observed. Through EDX point analysis, the lighter regions (3, 4, and 5 in **Figure 2**(d)) were identified as Mg_2(Si, Ge) and the darker regions (e.g. 1 and 2) corresponded to Si and Mg_2Si, as shown in Table 2. The white particles in images (f) and (h) were found to be Sn, in agreement with the XRD results.

The grain size was estimated using ImageJ to be 4.35 μm for $z = 0.1$ and 4.48 μm for $x = 0.2$ respectively. At least 20 grains were measured in order to estimate a reliable average on the grain size. The grain size measured for $z = 0.1$ and $x = 0.2$ is in the range of 4 – 5 μm which is the typical grain size obtained for the Mg_2X material systems and therefore presumably representative for all our samples [14, 20, 38].

3.2 Thermoelectric properties of p-type $Mg_{2-y}Li_yGe_{1-z}Si_z$

Table 3 List of $Mg_{2-y}Li_yGe_{1-z}Si_z$ samples with nominal composition, carrier concentration, Hall mobility and lattice constant. The carrier concentration and Hall mobility are calculated as effective quantities using a single parabolic band (SPB) model.

Composition	$p_H \times 10^{19}(cm^{-3})$	μ_H (cm^2/Vs)	ρ (g/cm^3)
$Mg_{1.99}Li_{0.01}Ge_{0.9}Si_{0.1}$	2.6	29.1	2.97
$Mg_{1.98}Li_{0.02}Ge_{0.9}Si_{0.1}$	3.3	25.7	2.97
$Mg_{1.97}Li_{0.03}Ge_{0.9}Si_{0.1}$	5.8	48.2	2.92
$Mg_{1.95}Li_{0.05}Ge_{0.9}Si_{0.1}$	3.0	28.6	2.96
$Mg_{1.98}Li_{0.02}Ge_{0.8}Si_{0.2}$	1.5	9.2	2.82
$Mg_{1.97}Li_{0.03}Ge_{0.8}Si_{0.2}$	1.6	39.1	2.85

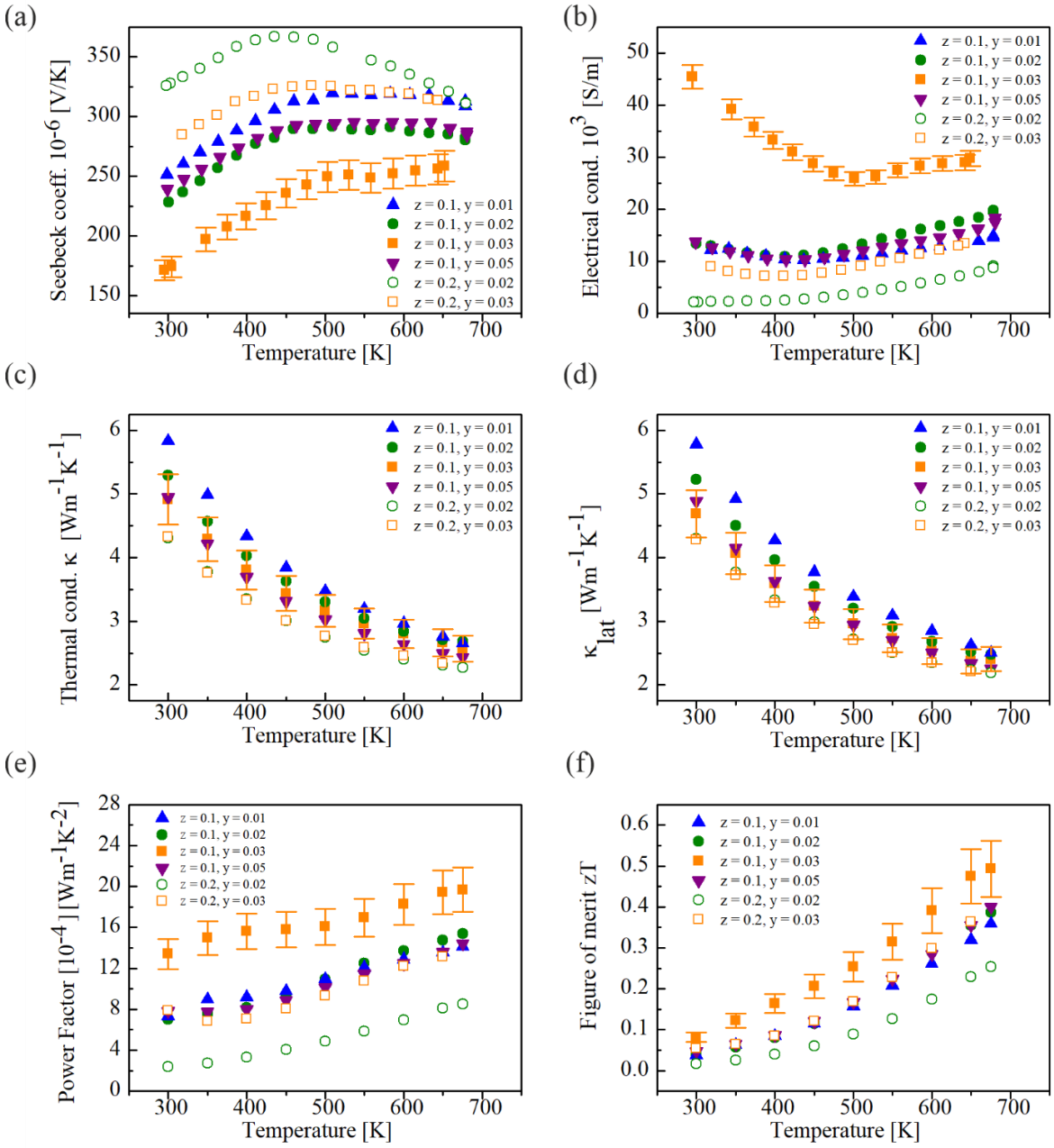

Figure 3 Temperature dependent (a) Seebeck coefficient, (b) electrical conductivity, (c) thermal conductivity, (d) lattice thermal conductivity, (e) power factor, and (f) figure of merit of $Mg_{1-y}Li_yGe_{1-z}Si_z$ with z = 0.1 and 0.2 and y = 0.02, and 0.03. In addition, y = 0.01 and 0.05 were for the z = 0.1.

In general, all samples show positive Seebeck coefficients corresponding to dominant hole conduction in the materials (**Figure 3a**). For $z = 0.1$, generally we observe that the Seebeck coefficient decreases as the Li content increases and that the trend is opposite for the electrical conductivity which is possibly due to the increase in carrier concentration and mobility as verified by the Hall measurement, except for $y = 0.05$. The Seebeck coefficient increases with temperature and almost becomes constant at around 500 K. For the electrical conductivity, we observe a decrease followed by a sharp increase as temperature increases. The rising in electrical conductivity initiates around 425 K for the $y = 0.01$ and $y = 0.02$ samples whereas in the case of $y = 0.03$, the rising is not as sharp as for the other samples and occurs at a higher temperature. The thermal conductivity and the lattice thermal conductivity show similar trends. The lattice thermal conductivity was estimated from $\kappa_{\mathrm{lat}} + \kappa_{\mathrm{bi}} = \kappa - L\sigma T$, where the Lorenz number (L) was estimated by employing a SPB model: $L = \left(\frac{k_b}{e}\right)^2 \frac{3F_0(\eta)F_2(\eta) - 4F_1^2(\eta)}{F_0(\eta)^2}$. We argue that $\kappa_{\mathrm{bi}} \approx 0$ due to the relatively large band gap of Mg_2Ge (and Ge-rich Mg_2X) and the arguments given in [20]. The influence of the primary thermoelectric properties can be seen in the trends observed for the power factor as the highest power factor value of 19.7×10^{-4} [$Wm^{-1}K^{-2}$] at 675 K was obtained for the $y = 0.03$ sample due to the significantly higher electrical conductivity. Thus, due to the high-power factor, the maximum zT is calculated to be 0.49 ± 0.07 at 675 K.

For $z = 0.2$ too, we observe that the Seebeck coefficient decreases as the Li content increases and that the trend is opposite for the electrical conductivity. Measurement of the transport properties of the $z = 0.2$ set of samples yielded a lot of complications with high resistivity being observed during the measurements and all the samples were re-measured. The samples were found to be thermally unstable and were also found to undergo oxidation during the measurements. The

Seebeck coefficient increases until 450 K and then decreases for $y = 0.02$ while it levels off at around 450 K for $y = 0.03$. The upturn point in electrical conductivity shifts towards lower temperatures as the carrier concentration is increased ($y = 0.02$ at around 450 K and $y = 0.03$ at around 425 K).

3.3 Thermoelectric properties of p-type $Mg_{2-y}Li_yGe_{1-x}Sn_x$

Table 4 List of $Mg_{2-y}Li_yGe_{1-x}Sn_x$ samples with nominal composition, carrier concentration, Hall mobility and lattice constant. The carrier concentration and Hall mobility are calculated as effective quantities using the SPB model.

Composition	$p_H \times 10^{19} (cm^{-3})$	μ_H (cm^2/Vs)	ρ (g/cm^3)
$Mg_{1.98}Li_{0.02}Ge_{0.9}Sn_{0.1}$	5.0	21.7	3.10
$Mg_{1.97}Li_{0.03}Ge_{0.9}Sn_{0.1}$	5.1	18.4	3.18
$Mg_{1.98}Li_{0.02}Ge_{0.8}Sn_{0.2}$	5.1	21.4	3.14
$Mg_{1.97}Li_{0.03}Ge_{0.8}Sn_{0.2}$	5.2	18.0	3.12

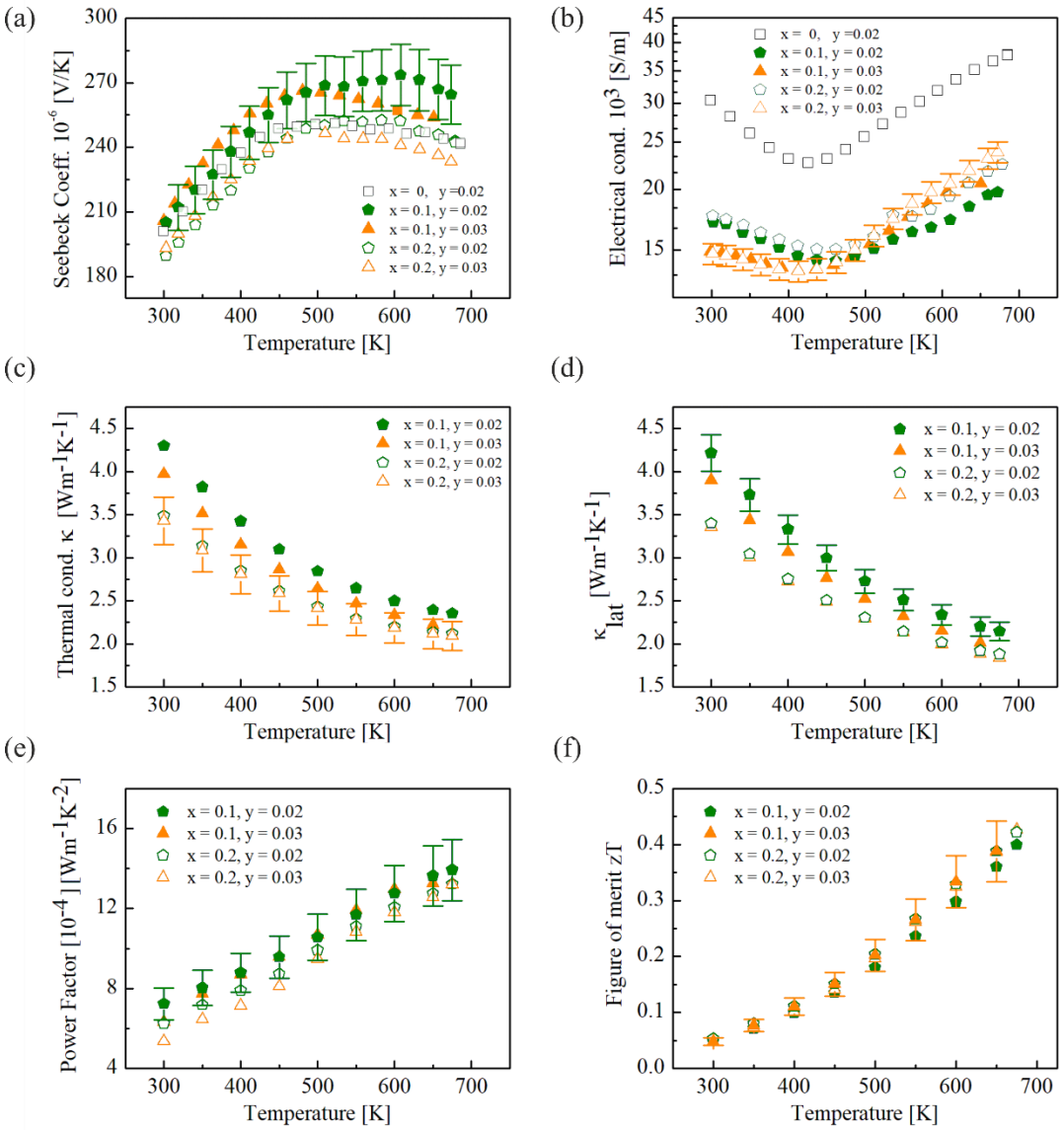

Figure 4 Temperature dependent (a) Seebeck Coefficient, (b) electrical conductivity, (c) thermal conductivity, (d) lattice thermal conductivity, (e) power factor, and (f) figure of merit of $Mg_{2-y}Li_yGe_{1-x}Sn_x$ with x = 0.1 and 0.2 and y = 0.02 and 0.03.

The Seebeck coefficient displays positive values and for x = 0.1, we observe that the Seebeck coefficient increases with increasing temperature and decreases at around 600 K for y = 0.02 and 450 K for y = 0.03 whereas for the electrical conductivity we observe a gradual decrease followed by a sharp increase which starts at around 475 K for y = 0.02 and 425 K for y = 0.03 **(Figure 4).** It should also be noted that the upturn observed in the electrical conductivity is much sharper for

y = 0.03. The comparable *S* and σ data agree with the relatively similar carrier concentrations and mobility values obtained from the Hall measurements. The temperature dependent Seebeck coefficient and electrical conductivity of $Mg_2Ge_{1-x}Sn_x$ is similar to the behavior of the Li doped Mg_2Ge (Figure 4a and b).

For $x = 0.2$, we notice that the Seebeck coefficient decreases gradually starting at around 500 K for y = 0.03 and 625 K for y = 0.02 while we see a considerable upturn in the electrical conductivity which starts at 425 K for y = 0.03 and 475 K for y = 0.02. The thermal conductivity and lattice thermal conductivity are in general lower for the x = 0.2 system due to the higher alloy scattering effect and the reduction observed is found to vary from 10% to 20 % throughout the whole temperature range. Thus, owing to the reduction in the thermal conductivity and the higher electrical conductivity observed, the maximum power factor value of 13 $\times 10^{-4}$ [$Wm^{-1}K^{-2}$] at 675 K is achieved for x = 0.2, y = 0.03 and thus a maximum zT of 0.43 ± 0.07 at 675 K is achieved for the same system.

4. Discussion

The XRD and Rietveld refinement results show the main phase and no elemental impurities for $Mg_2Ge_{0.9}Si_{0.1}$ while a number of secondary phases corresponding to Mg_2Ge, Mg_2Si, $Mg_2Ge_{0.88}Si_{0.09}$, and $Mg_2Ge_{0.46}Si_{0.16}$ were obtained for the $Mg_2Ge_{0.8}Si_{0.2}$. The SEM images also depict unreacted Si for $z = 0.2$ indicating an incomplete reaction of Mg, Si, and Ge. Whereas for $x = 0.1$ and 0.2, white particles corresponding to unreacted Sn are observed with SEM-EDX and Rietveld refinement as well (see supporting information). The presence of unreacted elements and secondary phases is possibly due to the differences in mechanical properties of Mg, Ge, Si, and Sn important for the solid state reaction during the milling process.

From the observation of large elemental Si particles (**Figure 2**(c) and (d)) it can be hypothesized for the $Mg_2(Ge,Si)$ system that the Mg_2Ge phase is thermodynamically more favorable than Mg_2Si, thus possibly allowing Si to diffuse into the matrix similar to what was found for $Mg_2(Si,Sn)$ [14]. This is supported by the fact that the formation energy of Mg_2Ge is found to be 35% larger than that of Mg_2Si with values corresponding to –104.25 kJ/mol and -68.85 kJ/mol, respectively at 298.15 K, with all values being calculated using Thermo-Calc and the TCAL6 database [39-40]. The calculated values were found to be comparable to those reported in literature [41-42]. Due to sample instability and increased inhomogeneity observed as the Si content increases, it can be concluded that investigating compositions with higher Si content would most likely not produce better results. Finally, it can be deduced that a more suitable microstructure can be expected with a further optimization of the synthesis parameters (milling time), especially for the $z = 0.2$ system.

With respect to the Sn containing samples, the small amounts of unreacted Sn observed on the $Mg_2Ge_{0.9}Sn_{0.1}$ and $Mg_2Ge_{0.8}Sn_{0.2}$ matrix might be due to incomplete diffusion or due to loss of Mg during the sintering step [14, 20, 25] shifting the phase equilibrium towards the Mg poor region where $Mg_2(Ge,Sn)$ and Sn coexist. The formation energy of Mg_2Ge is found to be 25% higher than that of Mg_2Sn (-76.980 kJ/mol), thus supporting the fact that the formation of Mg_2Ge is thermodynamically more favorable and Sn might subsequently diffuse into the system; this hypothesis requires verification by experiments performed with longer milling times. Similarly, previous work by Sankhla et al.[14] on the $Mg_2(Si,Sn)$ system highlighted the fact that milling for longer times decreases the extent of elemental impurities being present. This would likely lead to a further improvement of the thermoelectric properties as they are correlated with microstructure and phase distribution.

Overall the temperature dependence of the electronic transport properties does not resemble that of typical, highly doped thermoelectric materials [16]. Instead, the characteristic features of a relatively sharp increase in electrical conductivity at low temperature and slight or no decrease of the Seebeck coefficient at high temperatures, match those of binary p-type Mg_2Ge [20] (**Figure 4**a and b). For p-type Mg_2Ge this has been explained with a strong temperature dependence of the valence bands and it is plausible that the same mechanism holds here. Thus, the almost constant Seebeck coefficient at higher temperatures and the decrease in electrical conductivity followed by a sharp increase, in Li doped $Mg_2Ge_{1-x}Sn_x$ and $Mg_2Ge_{1-z}Si_z$ are possibly due to the movement of the split off (SO) band whose energetic difference decreases with increasing temperature [20].

The comparison of the behavior of the Seebeck coefficient and electrical conductivity of undoped Mg_2Ge in Figure S3 clearly demonstrates the influence of Li doping on the material systems tested in this work; the increased charge carrier concentration is in full agreement with our earlier work [20]. The undoped Mg_2Ge sample shows indications for mixed conduction and transitions from p-type to n-type above room temperature while Li-doped samples exhibit dominant hole conduction due to an enhanced hole concentration.

From the changes of carrier concentration with increasing x or z it can be deduced that the dopant efficiency (measured carrier concentration over Li concentration) is generally relatively low and decreases with increasing Si content and with increasing Li content whereas it seems to remain constant for Sn compositions. The values lie around 0.2 for the binary Mg_2Ge system [20] and x = 0.1, 0.2, whereas with the addition of Si the dopant efficiency reduces to around 0.1 for $z = 0.1$ and 0.2. The dopant efficiency for p-type Mg_2Si was found to be even lower [16] and it is unlikely that this changes non-monotonously with composition.

A possible explanation is that Li occupies both Mg and interstitial sites thus serving simultaneously as a p-type and an n-type dopant. Previous report by Gao et al [18], suggests that Li can easily occupy both Mg (Li_{Mg}) substitutional and interstitial sites (Li_{int}) and it has also been noted by Kumari et al.[43] and Ayachi et al. [44], that the formation energy is lowest when Li occupies the Mg interstitial positions. These results from calculations are in contradiction to the experimental report by Nieroda et al [45], which states that Li occupancy at the Mg site is more favorable. Nevertheless, Li might be self-compensating, explaining the overall low dopant efficiency, while the balance between $Li_{Mg}$and Li_{int} might depend on the Si:Ge:Sn ratio.

We have also observed a minor change in the first measurement cycle which later becomes stable (Figure S2). The effect of the observed secondary phases can be estimated, in particular as these form only non-connected islands. Si can be expected to have a much lower electrical conductivity, possibly coming from a reduction of the mobility of the charge carriers. Elemental Sn is metallic but as the Sn-islands are sub-µm sized, they also probably act as scattering centers. As the dopant efficiency decreases with increasing Si-content in Mg_2(Ge,Si), Mg_2Si or Si-richer Mg_2(Ge,Si) can likewise be expected to behave as lower doped particles, causing mainly a reduction in carrier mobility, similar to what has been previously observed in [38].

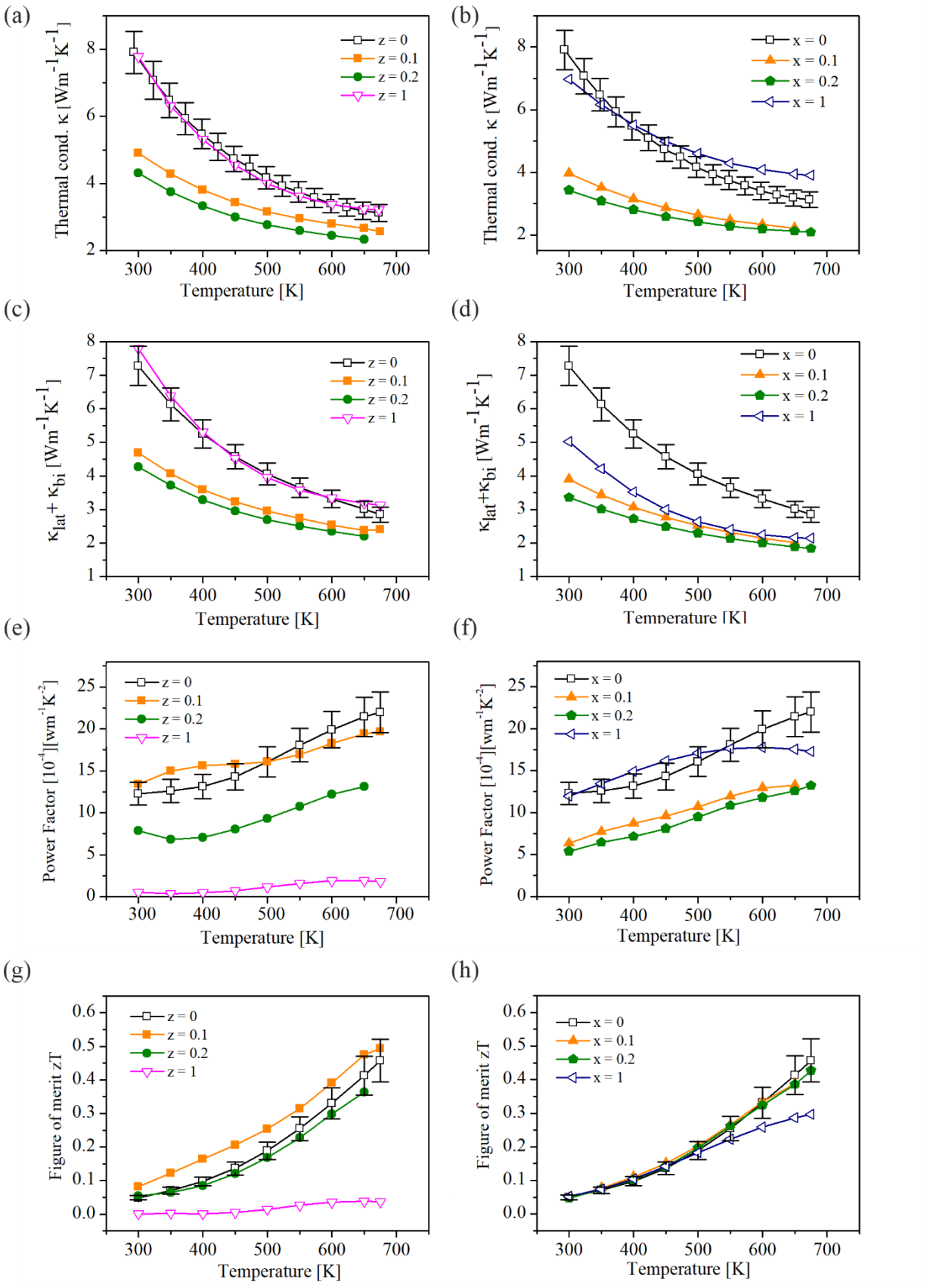
(a)
Thermal cond. κ [Wm^{-1}K^{-1}]
Temperature [K]
z = 0
z = 0.1
z = 0.2
z = 1
(b)
Thermal cond. κ [Wm^{-1}K^{-1}]
Temperature [K]
x = 0
x = 0.1
x = 0.2
x = 1
(c)
$\kappa_{lat}+\kappa_{bi}$ [Wm^{-1}K^{-1}]
Temperature [K]
z = 0
z = 0.1
z = 0.2
z = 1
(d)
$\kappa_{lat}+\kappa_{bi}$ [Wm^{-1}K^{-1}]
Temperature [K]
x = 0
x = 0.1
x = 0.2
x = 1
(e)
Power Factor [10^{-4}][wm^{-1}K^{-2}]
Temperature [K]
z = 0
z = 0.1
z = 0.2
z = 1
(f)
Power Factor [10^{-4}][wm^{-1}K^{-2}]
Temperature [K]
x = 0
x = 0.1
x = 0.2
x = 1
(g)
Figure of merit zT
Temperature [K]
z = 0
z = 0.1
z = 0.2
z = 1
(h)
Figure of merit zT
Temperature [K]
x = 0
x = 0.1
x = 0.2
x = 1

Figure 5 Thermoelectric properties of $Mg_{2-y}Li_yGe_{1-z}Si_z$ and $Mg_{2-y}Li_yGe_{1-x}Sn_x$ where x and $z = 0 - 1$. Li concentration ($y = 0.02\ or\ 0.03$) was taken from the sample with the best overall thermoelectric properties and was y = 0.02 or 0.03. Temperature dependent (a-b) thermal conductivity, (c-d) lattice thermal conductivity, (e – f) power factor and (g-h) figure of merit for different Li concentrations compared with literature from [16, 19-20, 36].

The effect of solid solution formation and the trends with increasing Si and Sn content can be discerned from **Figure 5**(a) which shows that the thermal conductivity decreases around 30% throughout the whole temperature range for $z = 0.1$ and 0.2 as compared to the binaries, most likely because of more scattering in the system. The addition of Si into the system creates an alloying effect and increases disorder in the system. For the power factor a reduction is expected as the scattering of the holes is also increased due to the alloying [46]. From the data available we find comparable power factors for Mg_2Ge and $Mg_2Ge_{0.9}Si_{0.1}$ with the Mg_2Ge being superior only at higher temperatures. The combined effect of κ_{lat} and PF lead to a higher zT for $z = 0.1$ compared to Mg_2Ge ($z = 0$) in a large temperature range. In the case of $Mg_2(Ge,Sn)$, we observe that the thermal conductivities decreases by ~35 % as compared to Mg_2Ge ($z = 0$) throughout the whole temperature range. However, as compared to Mg_2Sn, the values are relatively similar for T>500 K. Furthermore, we observe that the power factor is significantly reduced compared to Mg_2Ge and thus overall, there is no improvement in zT.

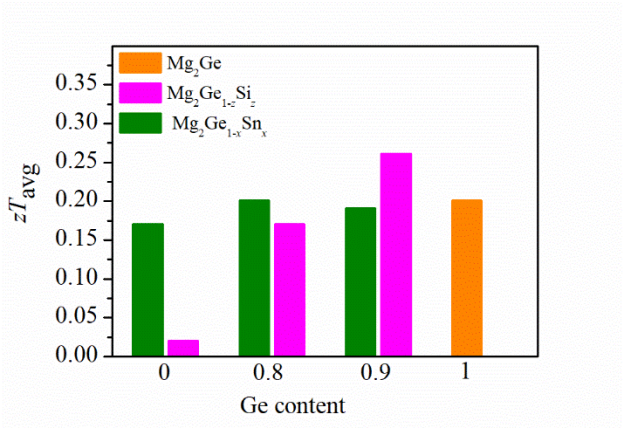

Figure 6 zT_{avg} calculated for between 300 K and 675 K (except for for z = 0.2 where $T_h = 650$ K was employed) along with literature comparison. [16, 20]

While materials are often compared with respect to their maximum figure of merit, the average figure of merit is much closely related to the expected device efficiency (η_{max}) [47-49]. The average zT was calculated by integrating the zT curve from the hot end (T_h) to the cold end (T_c)[47, 49], where $T_h = 675$ K and $T_c = 300$ K for all samples except z = 0.2 and $x = 0.1$ ($T_h = 650$ K) (**Figure 6**).

For $z = 0$ and $z = 0.1$, zT_{avg} values of 0.20 and 0.26 were obtained respectively while with $x = 0.1$ and $x = 0.2$ systems, we obtain zT_{avg} values of 0.19 and 0.20. In principle, we see that there is an increase of ~30% for the z = 0.1 system as compared to the binary Mg_2Ge system whereas for the Sn containing samples we do not observe a significant improvement. We don't expect further improvement for Si-richer compositions in the Mg_2Si-Mg_2Ge system due to material instability and low dopant efficiency.

5. Conclusion

The first reported syntheses of p-type $Mg_{2-y}Li_yGe_{1-z}Si_z$ and $Mg_{2-y}Li_yGe_{1-x}Sn_x$ with x, z = 0.1 and 0.2 using Li as a dopant were carried out via high energy ball milling and direct current sintering. No MgO was observed in all samples, however the presence of elemental Sn and Mg_2Sn was observed for $x = 0.1$ and 0.2 through XRD, Rietveld refinement, and SEM/EDX studies. In addition, several secondary phases corresponding to Si and Ge rich phases were observed for z = 0.2 through SEM and Rietveld refinement. Our results indicate that milling time should be increased with increasing substitution of Ge by Si/Sn. We further observe unusual temperature dependent electronic transport data, of S and σ, which are similar to those of binary p-type Mg_2Ge.

Li was identified as suitable p-type dopant but the dopant efficiency was found to decrease with increasing Si content. The thermal conductivity decreases significantly (~ 30%) by alloying which compensates for the decrease in carrier mobility observed due to alloy scattering. A maximum *zT* value of 0.49 was obtained at 675 K for z = 0.1 which currently lies in the range of best values for Ge rich Mg_2(Si, Ge, Sn) solid solutions. More importantly the average *zT* of 0.26 was found to be 30 % higher than that of binary Mg_2Ge. Furthermore, a maximum *zT* value of 0.43 and average *zT* value of 0.20 were obtained for $x = 0.2$ which is comparable to that of binary Mg_2Ge.

Acknowledgements

We would like to gratefully acknowledge the endorsement from the DLR Executive Board Members for Space Research and Technology and the financial support from the Young Research Group Leader Program. The authors would like to thank to P. Blaschkewitz (DLR) for his continuous support with the thermoelectric measurements. The authors (H.K. and A.S.) would like to acknowledge financial support by the DAAD (Fellowships no. 247). The authors would like to acknowledge G.C Hernandez for help with the sample preparation for SEM/EDS measurements. M. Yasseri would like to thank for financial support provided by the DFG via the RTG (Research Training Group) 2204 "Substitute Materials for Sustainable Energy Technologies" at JLU Gießen.

References

1. Bell, L. E., Cooling, Heating, Generating Power, and Recovering Waste Heat with Thermoelectric Systems. *Science* **2008,** *321* (5895), 1457-1461.
2. Snyder, G. J.; Toberer, E. S., Complex thermoelectric materials. *Nature Materials* **2008,** *7* (2), 105-114.
3. Pei, Y.; Shi, X.; LaLonde, A.; Wang, H.; Chen, L.; Snyder, G. J., Convergence of electronic bands for high performance bulk thermoelectrics. *Nature* **2011,** *473* (7345), 66-69.
4. Liu, W.; Tan, X.; Yin, K.; Liu, H.; Tang, X.; Shi, J.; Zhang, Q.; Uher, C., Convergence of conduction bands as a means of enhancing thermoelectric performance of n-type $Mg_2Si_{1-x}Sn_x$ solid solutions. *Physical review letters* **2012,** *108* (16), 166601.
5. Zhang, Q.; Cao, F.; Liu, W.; Lukas, K.; Yu, B.; Chen, S.; Opeil, C.; Broido, D.; Chen, G.; Ren, Z., Heavy doping and band engineering by potassium to improve the thermoelectric figure of merit in p-type PbTe, PbSe, and $PbTe_{1-y}Sey$. *Journal of the American chemical society* **2012,** *134* (24), 10031-10038.

6. Heremans, J. P.; Wiendlocha, B.; Chamoire, A. M., Resonant levels in bulk thermoelectric semiconductors. *Energy & Environmental Science* **2012,** *5* (2), 5510-5530.
7. Liu, W.; Kim, H. S.; Chen, S.; Jie, Q.; Lv, B.; Yao, M.; Ren, Z.; Opeil, C. P.; Wilson, S.; Chu, C.-W.; Ren, Z., n-type thermoelectric material Mg2Sn0. 75Ge0. 25 for high power generation. *Proceedings of the National Academy of Sciences* **2015,** *112* (11), 3269-3274.
8. Wu, D.; Zhao, L.-D.; Tong, X.; Li, W.; Wu, L.; Tan, Q.; Pei, Y.; Huang, L.; Li, J.-F.; Zhu, Y.; Kanatzidis, M. G.; He, J., Superior thermoelectric performance in PbTe–PbS pseudo-binary: extremely low thermal conductivity and modulated carrier concentration. *Energy & Environmental Science* **2015,** *8* (7), 2056-2068.
9. Yu, C.; Zhu, T.-J.; Shi, R.-Z.; Zhang, Y.; Zhao, X.-B.; He, J., High-performance half-Heusler thermoelectric materials Hf_{1-x} Zr_xNiSn$_{1-y}$Sby prepared by levitation melting and spark plasma sintering. *Acta Materialia* **2009,** *57* (9), 2757-2764.
10. Hu, X.; Jood, P.; Ohta, M.; Kunii, M.; Nagase, K.; Nishiate, H.; Kanatzidis, M. G.; Yamamoto, A., Power generation from nanostructured PbTe-based thermoelectrics: comprehensive development from materials to modules. *Energy & Environmental Science* **2016,** *9* (2), 517-529.
11. Qiu, Y.; Xi, L.; Shi, X.; Qiu, P.; Zhang, W.; Chen, L.; Salvador, J. R.; Cho, J. Y.; Yang, J.; Chien, Y. c., Charge-compensated compound defects in Ga-containing thermoelectric skutterudites. *Advanced Functional Materials* **2013,** *23* (25), 3194-3203.
12. Yan, X.; Joshi, G.; Liu, W.; Lan, Y.; Wang, H.; Lee, S.; Simonson, J.; Poon, S.; Tritt, T.; Chen, G.; Ren, Z., Enhanced thermoelectric figure of merit of p-type half-Heuslers. *Nano Letters* **2011,** *11* (2), 556-560.
13. Zhang, J.; Song, L.; Pedersen, S. H.; Yin, H.; Iversen, B. B., Discovery of high-performance low-cost n-type Mg_3Sb_2-based thermoelectric materials with multi-valley conduction bands. *Nature communications* **2017,** *8* (1), 1-8.
14. Sankhla, A.; Patil, A.; Kamila, H.; Yasseri, M.; Farahi, N.; Mueller, E.; de Boor, J., Mechanical alloying of optimized Mg_2 (Si, Sn) solid solutions: understanding phase evolution and tuning synthesis parameters for thermoelectric applications. *ACS Applied Energy Materials* **2018,** *1* (2), 531-542.
15. Goyal, G. K.; Mukherjee, S.; Mallik, R. C.; Vitta, S.; Samajdar, I.; Dasgupta, T., High Thermoelectric Performance in Mg_2 ($Si_{0.3}Sn_{0.7}$) by Enhanced Phonon Scattering. *ACS Applied Energy Materials* **2019,** *2* (3), 2129-2137.
16. Kamila, H.; Sahu, P.; Sankhla, A.; Yasseri, M.; Pham, H.-N.; Dasgupta, T.; Mueller, E.; de Boor, J., Analyzing transport properties of p-type Mg_2Si–Mg_2Sn solid solutions: optimization of thermoelectric performance and insight into the electronic band structure. *Journal of Materials Chemistry A* **2019,** *7* (3), 1045-1054.
17. de Boor, J.; Dasgupta, T.; Saparamadu, U.; Mueller, E.; Ren, Z., Recent progress in p-type thermoelectric magnesium silicide based solid solutions. *Materials today energy* **2017,** *4*, 105-121.
18. Gao, P.; Davis, J. D.; Poltavets, V. V.; Hogan, T. P., The p-type Mg_2 Li_x $Si_{0.4}$ $Sn_{0.6}$ thermoelectric materials synthesized by a B_2O_3 encapsulation method using Li_2CO_3 as the doping agent. *Journal of Materials Chemistry C* **2016,** *4* (5), 929-934.
19. Saparamadu, U.; de Boor, J.; Mao, J.; Song, S.; Tian, F.; Liu, W.; Zhang, Q.; Ren, Z., Comparative studies on thermoelectric properties of p-type $Mg_2Sn_{0.75}Ge_{0.25}$ doped with lithium, sodium, and gallium. *Acta Materialia* **2017,** *141*, 154-162.
20. Kamila, H.; Sankhla, A.; Yasseri, M.; Mueller, E.; de Boor, J., Non-Rigid Band Structure in Mg_2Ge for Improved Thermoelectric Performance. *Advanced Science 7* (12), 2000070.
21. Kamila, H.; Goyal, G. K.; Sankhla, A.; Ponnusamy, P.; Mueller, E.; Dasgupta, T.; de Boor, J., Systematic analysis of the interplay between synthesis route, microstructure, and thermoelectric performance in p-type $Mg_2Si_{0.2}Sn_{0.8}$. *Materials Today Physics* **2019**, 100133.
22. Kolezynski, A.; Nieroda, P.; Wojciechowski, K. T., Li doped Mg_2Si p-type thermoelectric material: theoretical and experimental study. *Computational Materials Science* **2015,** *100*, 84-88.
23. Akasaka, M.; Iida, T.; Matsumoto, A.; Yamanaka, K.; Takanashi, Y.; Imai, T.; Hamada, N., The thermoelectric properties of bulk crystalline n-and p-type Mg_2 Si prepared by the vertical Bridgman method. *Journal of Applied Physics* **2008,** *104* (1), 013703.
24. An, T.-H.; Park, C.; Seo, W.-S.; Choi, S.-M.; Kim, I.-H.; Kim, S.-U., Enhancement of p-type thermoelectric properties in an Mg 2 Sn system. *Journal of the Korean Physical Society* **2012,** *60* (10), 1717-1723.
25. Kamila, H.; Sankhla, A.; Yasseri, M.; Hoang, N. P.; Farahi, N.; Mueller, E.; de Boor, J., Synthesis of p-type $Mg_2Si_{1-x}Snx$ with x = 0-1 and optimization of the synthesis parameters. *Materials Today: Proceedings* **2019,** *8*, 546-555.

26. de Boor, J.; Stiewe, C.; Ziolkowski, P.; Dasgupta, T.; Karpinski, G.; Lenz, E.; Edler, F.; Mueller, E., High-temperature measurement of Seebeck coefficient and electrical conductivity. *Journal of electronic materials* **2013,** *42* (7), 1711-1718.
27. Ziolkowski, P.; Stiewe, C.; de Boor, J.; Druschke, I.; Zabrocki, K.; Edler, F.; Haupt, S.; König, J.; Mueller, E., Iron disilicide as high-temperature reference material for traceable measurements of Seebeck coefficient between 300 K and 800 K. *Journal of Electronic Materials* **2017,** *46* (1), 51-63.
28. Borup, K. A.; de Boor, J.; Wang, H.; Drymiotis, F.; Gascoin, F.; Shi, X.; Chen, L.; Fedorov, M. I.; Mueller, E.; Iversen, B. B., Measuring thermoelectric transport properties of materials. *Energy & Environmental Science* **2015,** *8* (2), 423-435.
29. Dinnebier, R. E.; Leineweber, A.; Evans, J. S., *Rietveld refinement: practical powder diffraction pattern analysis using TOPAS*. Walter de Gruyter GmbH & Co KG: 2018.
30. Van der Pauw, L. J., A Method of Measuring the Resistivity and Hall Coefficient on Lamellae of Arbitrary Shape. *Philips Tech. Rev* **1958,** *20*, 220-224.
31. de Boor, J., On the applicability of the single parabolic band model to advanced thermoelectric materials with complex band structures. *Journal of Materiomics* **2021,** *7* (3), 603-611.
32. Aizawa, T.; Song, R.; Yamamoto, A., Solid-state synthesis of thermoelectric materials in Mg–Si–Ge system. *Materials transactions* **2005,** *46* (7), 1490-1496.
33. LaBotz, R. J.; Mason, D. R., The thermal conductivities of Mg_2Si and Mg_2Ge. *Journal of The Electrochemical Society* **1963,** *110* (2), 121.
34. Zaitsev, V. K.; Fedorov, M.; Gurieva, E. A.; Eremin, I. S.; Konstantinov, P. P.; Samunin, A.; Vedernikov, M. V., *Thermoelectrics of n-type with ZT > 1 based on Mg_2Si-Mg2Sn solid solutions*. 2005; Vol. 2005, p 204-210.
35. Noda, Y.; Kon, H.; Furukawa, Y.; Otsuka, N.; Nishida, I. A.; Masumoto, K., Preparation and Thermoelectric Properties of Mg2Ge1-xSix Solid Solution Semiconductors. *Materials Transactions, JIM* **1992,** *33* (9), 845-850.
36. de Boor, J.; Saparamadu, U.; Mao, J.; Dahal, K.; Mueller, E.; Ren, Z., Thermoelectric performance of Li doped, p-type Mg_2 (Ge, Sn) and comparison with Mg2 (Si, Sn). *Acta Materialia* **2016,** *120*, 273-280.
37. Somasundaram, T., Radiation Contaminations in Powder X-Ray Diffraction (PXRD) Patterns. **2015,** *Radiation Contaminations in Powder X-Ray Diffraction (PXRD) Patterns Version: 20151109*.
38. Kamila, H.; Goyal, G. K.; Sankhla, A.; Ponnusamy, P.; Mueller, E.; Dasgupta, T.; de Boor, J., Systematic analysis of the interplay between synthesis route, microstructure, and thermoelectric performance in p-type $Mg_2Si_{0.2}Sn_{0.8}$. *Materials Today Physics* **2019,** *9*, 100133.
39. Andersson, J.; Helander, T.; Hoglund, L.; Shi, P.; Sundman, B., Calphad-Computer Coupling of Phase Diagrams and Thermochemistry. *Calphad* **2002,** *26*, 273.
40. Andersson, J.-O.; Helander, T.; Höglund, L.; Shi, P.; Sundman, B., Thermo-Calc & DICTRA, computational tools for materials science. *Calphad* **2002,** *26* (2), 273-312.
41. Clark, C.; Wright, C.; Suryanarayana, C.; Baburaj, E. G.; Froes, F. H., Synthesis of Mg_2X (X= Si, Ge, or Sn) intermetallics by mechanical alloying. *Materials Letters* **1997,** *33* (1-2), 71-75.
42. Jung, I.-H.; Kang, D.-H.; Park, W.-J.; Kim, N. J.; Ahn, S., Thermodynamic modeling of the Mg–Si–Sn system. *Calphad* **2007,** *31* (2), 192-200.
43. Kumari, A.; Nag, A.; Kumar, J., Ab-initio study of electronic and structural properties of lithium doped Mg2Si. *AIP Conference Proceedings* **2019,** *2142* (1), 110001.
44. Ayachi, S.; Deshpande, R.; Ponnusamy, P.; Park, S.; Chung, J.; Park, S.; Ryu, B.; Mueller, E.; de Boor, J., On the Relevance of Point Defects for the Selection of Contacting Electrodes: Ag as an Example for Mg_2(Si,Sn)-based Thermoelectric Generators. *Materials Today Physics* **2020**, 100309.
45. Nieroda, P.; Kolezynski, A.; Oszajca, M.; Milczarek, J.; Wojciechowski, K. T., Structural and Thermoelectric Properties of Polycrystalline p-Type $Mg_{2-x}Li_xSi$. *Journal of Electronic Materials* **2016,** *45* (7), 3418-3426.
46. Wang, H.; LaLonde, A. D.; Pei, Y.; Snyder, G. J., The Criteria for Beneficial Disorder in Thermoelectric Solid Solutions. *Advanced Functional Materials* **2013,** *23* (12), 1586-1596.
47. Ponnusamy, P.; de Boor, J.; Mueller, E., Using the constant properties model for accurate performance estimation of thermoelectric generator elements. *Applied Energy* **2020,** *262*, 114587.
48. Armstrong, H.; Boese, M.; Carmichael, C.; Dimich, H.; Seay, D.; Sheppard, N.; Beekman, M., Estimating Energy Conversion Efficiency of Thermoelectric Materials: Constant Property Versus Average Property Models. *J. Electron. Mater.* **2017,** *46* (1), 6-13.
49. Kim, H. S.; Liu, W.; Chen, G.; Chu, C.-W.; Ren, Z., Relationship between thermoelectric figure of merit and energy conversion efficiency. *Proceedings of the National Academy of Sciences* **2015,** *112* (27), 8205-8210.

"Optimization of the thermoelectric properties of p-type $Mg_{2-y}Li_yGe_{1-x}Sn_x$ and $Mg_{2-y}Li_yGe_{1-z}Si_z$ with x, z = 0.1 and 0.2.

Vidushi Galwadu Arachchige, Hasbuna Kamila*, Aryan Sankhla, Leo Millerand, Silvana Tumminello, Kunal Mitra, Mohammad Yasseri, Eckhard Müller, and Johannes de Boor**

Keywords : Synthesis, ball milling, p-type $Mg_2Ge_{1-z}Si_z$ solid solutions, p-type $Mg_2Ge_{1-x}Sn_x$ solid solutions, thermoelectric properties, microstructure

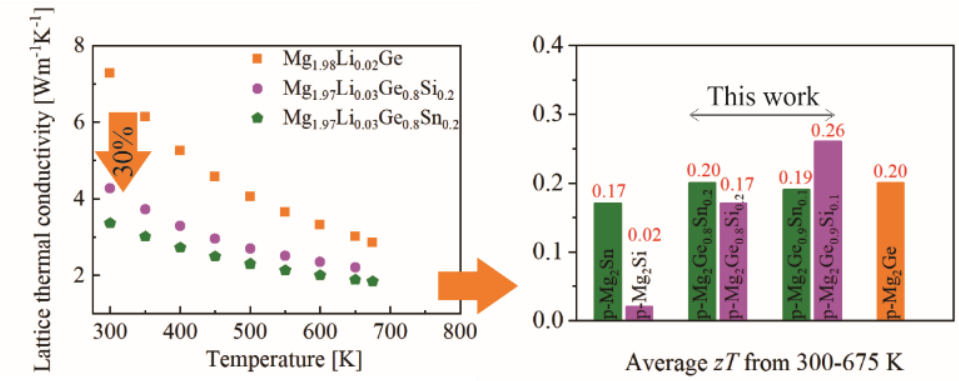

Alloying of Si or Sn into the Ge site of p-type $Mg_2Ge_{1-x}Sn_x$ and $Mg_2Ge_{1-z}Si_z$ with x, z = 0.1 and 0.2 leads to a 30% decrease in the lattice thermal conductivity. Furthermore, a 30% increase in average zT values are achieved as compared with p-type Mg_2Ge binary.